Engineering Structures 125 (2016) 1–14

Contents lists available at ScienceDirect

Engineering Structures

journal homepage: www.elsevier.com/locate/engstruct

Finite element modeling of FRP-confined concrete using modified concrete damaged plasticity

Najwa F. Hany, Elie G. Hantouche, Mohamed H. Harajli *

Department of Civil and Environmental Engineering, American University of Beirut, Lebanon

ARTICLE INFO

Article history:
Received 7 July 2015
Revised 23 June 2016
Accepted 28 June 2016

Keywords:
Concrete
Columns
Confinement
Fiber reinforced polymer
Finite element method
Plasticity

ABSTRACT

Finite element (FE) modeling of confined concrete columns is a challenging task because it requires accurate definition of the concrete material model to represent the volumetric behavior of concrete subject to triaxial stress states. When concrete is confined by fiber-reinforced polymer (FRP) composites, the problem becomes more complex due to the passive nature of the FRP confinement. Concrete Damaged Plasticity Model (CDPM) available in the finite element software package (ABAQUS) has been widely used to model reinforced concrete columns under axial stress. However, the use of CDPM has limitations when applied to confined concrete. This paper addresses these limitations and presents a modified Concrete Damaged Plasticity Model. A new set of strain hardening/softening constitutive relationships for both actively confined concrete and FRP-confined concrete are generated and a concrete dilation model is developed. The dilation model is expressed as a function of the stiffness of the FRP-jacket. The modified CDPM is applicable to columns with different types of cross-sections, including circular, square and rectangular and large range of concrete strengths varying from normal to high strength. Finite Element results obtained using the developed modified CDPM showed a very good agreement with test data for FRP confined concrete columns reported in the technical literature.

1. Introduction

During the last two decades, several experimental and analytical work has been carried out for evaluating the behavior of concrete columns confined with fiber reinforced polymer (FRP) composites when subjected to monotonic axial compressive loading. As a result, many stress-strain models have been developed, the majority of which were closed-form expressions calibrated based on available test data. Recent studies reviewed and assessed these available models [1–5]. FRP-confined concrete columns were also tested under axial cyclic loading and expressions to predict the cyclic response were also derived [6–9].

Further to the experimental and analytical work, many attempts have been made to model FRP-confined concrete columns using the Finite Element (FE) method. The main advantage of the FE method is its ability to deal with geometric non-linearity and the interactions of different materials. However, the main complexity of the FE modeling lies in the proper definition of the different materials properties (i.e. FRP sheets and concrete). FRP laminates are usually modeled as linear elastic materials. When the fibers are in the hoop directions, only the hoop properties are crucial. On the other hand, many constitutive models were suggested to define concrete properties in FE software, especially for concrete subjected to confinement pressure. The theory of plasticity has been widely used to model confined concrete. The first types of concrete plasticity models were based on: nonlinear elasticity, endo-chronic plasticity, classical plasticity, multi-laminate or micro-plane plasticity, and bounding surface plasticity. However, as reported by Mirmiran et al. [10], these models are either of limited applicability or require large number of parameters to be calibrated.

More recently, Drucker-Prager (D-P) type was one of the most used types of plasticity models for modeling confined concrete [11–21]. Studies using the D-P type plasticity model reported good results when predicting the monotonic behavior of FRP confined concrete. Among these studies, Rousakis et al. [21] was the first approach proposing closed-form equations that interrelate all the parameters of D-P model for concrete uniformly confined with FRP. These parameters included hardening/softening function, plastic potential function, dilation parameter, damage parameter. A failure criterion for FE analyses of circular columns was also proposed. This criterion validated the dependency of the concrete strength on the jacket rigidity and the fiber modulus of elasticity

* Corresponding author at: Department of Civil and Environmental Engineering, American University of Beirut, P.O. Box 11-0236, Riad El-Solh/Beirut 1107 2020, Lebanon.

E-mail address: mharajli@aub.edu.lb (M.H. Harajli).

http://dx.doi.org/10.1016/j.engstruct.2016.06.047
0141-0296/

that was suggested by many researchers [1–9,22]. The findings of Rousakis et al. [21] were utilized by Karabinis et al. [14] to calibrate the D-P model available in ABAQUS [23] to analyze concrete cylinders and concrete prisms with or without steel reinforcement. More recently, Jiang and Wu [12] used experimental results available in the literature to generate expressions of the plastic dilation angle β, friction angle φ and hardening/softening functions k required by a D-P type plasticity model for modeling FRP confined circular concrete. These expressions were implemented in ABAQUS [23] and were able to reproduce the experimental axial stress-strain responses of FRP confined normal strength concrete specimens subjected to compressive loading. Jiang and Wu [20] built on the findings of [12] and used a larger experimental database to determine the yield of concrete under a three-dimensional stress state. Their approach consisted of decoupling the friction angle and cohesion from the yield function and generating models for the different parameters using compression results. The research also studied the interrelation between the yield function and the potential function parameters and proposed a test methodology to plot the yield surface at any Lode angle.

Other researches modeled FRP-confined concrete using a Karagozian and Case (K-C) type plasticity model [24]. In 2010, Yu et al. [11] assessed existing D-P type plasticity models and proposed criteria for the yield function, hardening/softening rule and flow rule that should be included in a D-P type plasticity model, to accurately predict the behavior of both actively and passively confined concrete. D-P model modified by Yu et al. [11] showed some limitations addressed in a companion paper [25] using modified damaged plasticity model available in ABAQUS [23]. This model was later improved by Teng et al. [26] to capture the three dimensional behavior of FRP and steel confined concrete columns. Kabir and Shafei [27] also used concrete damage plasticity combined with smooth cap plasticity to model FRP-confined circular RC columns subjected to eccentric axial loading. A recent study by Ozbakkaloglu et al. [28] published during the review process of this paper, proposed a modified concrete damaged plasticity model for FRP-confined concrete of both normal and high strengths.

Furthermore, Lo et al. [29] proposed an FE model for FRP-confined rectangular concrete columns based on the concrete constitutive model developed by Dong et al. [30] and the failure surface of Menétrey and Willam [31].

Concrete damaged plasticity model (CDPM) available in ABAQUS [23], developed by Lubliner et al. [32] and modified by Lee and Fenves [33], although widely used to model reinforced concrete, shows limitations when modeling either concrete confined with a constant confinement pressure or FRP-confined concrete.

In this paper, the influence of the different input parameters of concrete damaged plasticity model (CDPM) on the monotonic behavior of FRP-confined concrete columns is studied. As a result, a modified CDPM is proposed to accurately predict the monotonic axial stress-axial strain responses of actively confined and FRP-confined concrete columns, as well as the lateral dilation of FRP-confined concrete. The approach adopted relies on calibrating the dilation angle and hardening/softening rule to respectively predict the theoretical lateral dilation of FRP-confined in circular sections and the stress-strain curves of actively confined concrete. Accordingly, new expressions of the dilation angle of FRP-confined concrete in circular sections and input hardening/softening rule of actively-confined concrete are generated. The dilation angle expression is generalized to the case of non-circular sections using Yu et al.'s [25] approach. As for the compression hardening data, the curves calibrated on actively-confined concrete are used as input material properties function of the confining pressure for FRP-confined concrete. The accuracy of the proposed model is validated against experimental results of fifteen carbon fiber reinforced polymer (CFRP) confined concrete specimens of different cross-section shape (circular, square and rectangular) experimentally tested by the same research group [9], and also against other experimental results available in the literature.

2. Concrete damaged plasticity model (CDPM)

In CDPM, the inelastic behavior of concrete is represented using the concepts of isotropic damaged elasticity together with isotropic tensile and compressive plasticity [23]. Within framework of damaged-plasticity, the effective stress tensor is defined as:

$$\bar{\sigma} = D : \sigma \tag{1}$$

where σ is the stress tensor and D is the damage tensor defined as:

$$D = \frac{1}{1-d} I \tag{2}$$

I being the identity matrix, and d the scalar stiffness degradation variable.

$\bar{\sigma}$ is also expressed as:

$$\bar{\sigma} = D_o^{el} : (\varepsilon - \varepsilon^{pl}) \tag{3}$$

where D_o^{el} is the initial (undamaged) elasticity matrix, and ε and ε^{pl} are respectively the total strain and the plastic strain tensors.

The main plasticity functions in CDPM include the *yield criterion* and the *flow function*.

The *yield criterion* defines the yield condition under multiaxial stress state and is defined as follows in terms of effective stresses:

$$F = \frac{1}{1-\alpha}(\bar{q} - 3\alpha\bar{p} + \beta(\widetilde{\varepsilon^{pl}})\langle -\hat{\bar{\sigma}}_{\min}\rangle - \gamma\langle \hat{\bar{\sigma}}_{\min}\rangle) - \bar{\sigma}_c(\widetilde{\varepsilon_c^{pl}}) = 0 \tag{4}$$

where $\alpha = \frac{f_{bo}/f'_c - 1}{2f_{bo}/f'_c - 1}$, $\beta = \frac{\overline{\sigma_c}(\widetilde{\varepsilon_c^{pl}})}{\overline{\sigma_t}(\widetilde{\varepsilon_t^{pl}})}(1-\alpha) - (1+\alpha)$, $\gamma = \frac{3(1-K_c)}{2K_c - 1}$.

In these equations, $\bar{p}$ and $\bar{q}$ are respectively the hydrostatic pressure expressed in terms of effective stress and the Mises equivalent effective stress; $\hat{\bar{\sigma}}_{\min}$ = minimum principal effective stress; $\langle\bullet\rangle$ is the Macauley bracket defined as $\langle x\rangle = \frac{1}{2}(|x| + x)$; f_{bo}/f'_c = ratio of the compressive strength under biaxial loading to uniaxial compressive strength; K_c = ratio of the second stress invariant on the tensile meridian to that on the compressive meridian at initial yield for any given value of the pressure invariant such that the minimum effective principal stress is positive. $\overline{\sigma_t}(\widetilde{\varepsilon_t^{pl}})$ and $\overline{\sigma_c}(\widetilde{\varepsilon_c^{pl}})$ are the effective tensile and compressive cohesion stresses respectively. $\overline{\sigma_c}(\widetilde{\varepsilon_c^{pl}})$ is the compressive strain-hardening/softening function that determines the evolution of the yield surface with the plastic deformation. $\widetilde{\varepsilon_t^{pl}}$ and $\widetilde{\varepsilon_c^{pl}}$ are respectively the tensile and compressive equivalent plastic strains. The compressive stresses and strains are considered positive and tensile stresses and strains are considered negative.

The *flow rule* determines the direction of plastic deformation and dictates the evolution of the plastic lateral to plastic axial strain increment. CDPM assumes a *non-associated potential plastic flow*:

$$\dot{\varepsilon}_{ij}^{p} = \eta \frac{\partial G}{\partial \overline{\sigma}_{ij}}, i,j = 1,2,3 \tag{5}$$

where G is the *flow potential function* defined as:

$$G = \sqrt{(e\sigma_{to}\tan\psi)^2 + \bar{q}^2} - \bar{p}\tan\psi \tag{6}$$

In this equation, e is the eccentricity, σ_{to} is the uniaxial tensile stress at failure, and ψ is the dilation angle.

The scalar stiffness degradation d is a function of a damage variable κ the evolution of which is controlled by the following equation [23]:

$$\dot{\kappa} = \eta H(\bar{\sigma}, \kappa) \tag{7}$$

The response is solution of Eqs. (3), (4), (5) and (7) that requires an iterative procedure.

Accordingly, in ABAQUS, the non-linear behavior of concrete is defined by the following features: *damage variable*, *yield criterion*, *hardening/softening rule* and *flow rule*.

The current definition of the damage-plasticity aspects, incorporated in ABAQUS [23], makes the *damage variable* and the *strain-hardening/softening rule* dependent on the plastic-deformation and the *flow rule* defined using constant parameters. The influence of each CDPM parameter on the behavior of FRP-confined concrete needs to be studied. The following section describes the FE modeling of an FRP-confined concrete specimen, i.e. the boundary conditions and interactions, element types and meshing, and material properties. The input parameters of CDPM, whose effect on FRP-confined concrete needs to be investigated through parametric study, are specified and the corresponding parametric studies are performed.

3. FE modeling

The general-purpose finite element program ABAQUS [23] is used to perform all the simulations.

3.1. Boundary conditions and interactions

Yu et al. [25] reported that for FRP-confined columns with length equal to twice the diameter, the effect of the end constraints on the behavior in the mid-height region of the column is negligible. Accordingly, Yu et al. [25] suggested modeling only a vertical slice rather than the full-scale specimen and to use axisymmetric boundary conditions for modeling circular section. In the current study, the axial stress-axial strain curve of a full-scale specimen fully wrapped with FRP, simulated in ABAQUS [23] assuming pinned ends, is compared to that of a slice with one end fixed against vertical translation and the second used to impose the applied load as a prescribed vertical displacement. Comparison between the two results shows minor difference and therefore, for computation efficiency, only a slice of the specimen will be modeled. Also, given the symmetry boundary conditions of the problem, only quarter the cross-section is modeled and symmetry boundary conditions are specified as shown in Figs. 1a and 2. For partially wrapped specimens with equally distributed FRP wraps, since the slice simplification cannot be used, and for computational efficiency, only half the height of the specimen was modeled with inclusion of symmetry boundary condition as shown in Fig. 1(b).

Tie constraint is used to model the interaction between FRP sheet and concrete, such that the nodes on both surfaces are constrained to displace similarly. This assumption is in accordance with Issa et al. [15] conclusion that the bond between concrete and FRP does not affect significantly the confinement behavior.

3.2. Element type and meshing

The FRP sheet is modeled as a shell element whereas the concrete core is modeled as a solid element. Four-node shell elements with reduced integration (S4R), and 8-node brick elements with three translation degrees of freedom at each node (C3D8R) are used to discretize the FRP sheets and concrete core, respectively. The mesh is refined to prevent any discontinuity in the stresses and strains distribution in the concrete core and the FRP-sheet, and a mesh convergence study is conducted to determine the optimal mesh size that provides accurate solution with reasonably short analysis time.

3.3. Material properties

3.3.1. FRP sheets

Under tensile loading, the FRP sheets demonstrate linear elastic behavior before brittle rupture at a stress equal to the ultimate rupture stress, f_{fu}. The FRP sheets properties are specified using "LAMINA" material type in which the modulus of elasticity E_1 in the hoop direction is defined in accordance with the value provided by the manufacturer; while $E_2,\ G_{12},\ G_{13}$ and G_{23} are assigned small values, and the Poisson's ratio ν is set equal to zero.

3.3.2. Concrete

The two parameters needed to describe the elastic behavior of concrete are the Poisson's ratio, ν_c, and the modulus of elasticity, E_c. When the modulus of elasticity is not measured experimentally, it is estimated according to ACI 318 [34] as $E_c = 4730\sqrt{f'_c}$ where f'_c is the unconfined concrete compressive strength expressed in MPa. The Poisson's ratio ν_c of concrete under uniaxial compressive stress ranges from 0.15 to 0.22, with a representative value of 0.19 or 0.20 [35]. A value of ν_c equal to 0.18 is adopted to perform the numerical simulations of test results if no experimental value is reported.

Accurate modeling of the plastic behavior of concrete requires precise definition of the three features: tensile behavior, compressive behavior and plasticity parameters.

3.3.2.1. Tensile behavior. Using CDPM, *tension stiffening* and *tension damage* data allow describing the tensile behavior of concrete. Since plain concrete specimens are modeled, *tension stiffening* is specified using the **CONCRETE TENSION STIFFENING, TYPE = GFI* option with the uniaxial tensile strength set equal to $0.1f'_c$. Zero tensile damage is assumed since only monotonic loading is considered. It should be noted that the selection of the tensile properties of concrete does not have a significant effect on the behavior of FRP-confined concrete columns given that these columns are subjected to triaxial compression.

3.3.2.2. Compressive behavior. The non-linear compressive behavior of concrete is divided into *compression hardening* and *compression damage*.

It has been widely stated in the literature that the compression hardening/softening rule is one of the most important parameters controlling the behavior of confined concrete when modeled using finite element [11,14,25,36]. The model proposed by Popovics [37] and adopted later by Mander et al. [38] to describe the uniaxial stress-strain curve of concrete is used in a first step to define the concrete compression hardening data and to perform parametric studies of specified CDPM parameters. However, it will be shown later that for confined specimens, a hardening/softening rule different from that used for unconfined specimens should be adopted. It is worth noting that Tao et al. [36] who modeled concrete-filled steel stub columns under monotonic loading also performed a parametric study to evaluate the influence of the different input parameters of CDPM on the axial stress-strain response of the columns.

However, the influence of the input strain/hardening softening rule on the lateral strain of FRP-confined concrete in circular specimens needs to be evaluated prior to selecting the input hardening/softening rule for performing the sensitivity analysis. Therefore, two similar circular specimens provided by the same confinement level were modeled. For one of these specimens, the

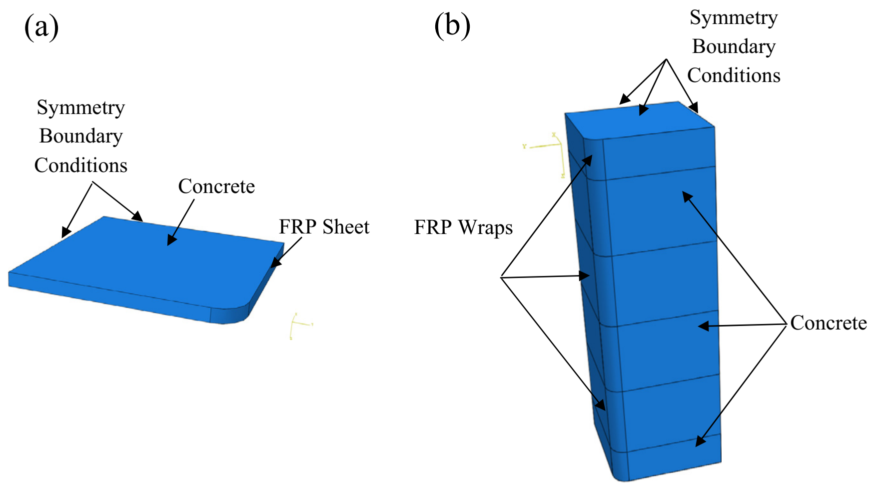

Fig. 1. Symmetry boundary conditions for square or rectangular specimens (a) fully wrapped, (b) partially wrapped.

input hardening/softening rule defined previously is adopted and for the second, the model of Popovics [37] is used to define the hardening/softening data before the peak stress while a perfectly plastic behavior is assumed after the peak stress. Comparison of the lateral strain in the FRP between these two specimens shows that it is almost the same but it is slightly reduced (after the first peak stress has been reached) when a perfectly plastic behavior is assumed. Therefore, the hardening/softening rule previously described is suitable for performing the parametric study.

Damage variable defines the degradation of the elastic stiffness during cyclic loading; however, its effect on the monotonic behavior of FRP-confined concrete columns is not clear. This effect is investigated through a parametric study that evaluates the influence of the compressive damage parameter, d_c, on the monotonic lateral strain-axial strain and axial stress-axial strain curves. The parametric study is performed on a circular specimen of radius $R = 100$ mm, unconfined compressive strength $f'_c = 18$ MPa and corresponding strain $\varepsilon_{co} = 0.002$, confined by a CFRP jacket of thickness $t_{frp} = 0.13$ mm and tensile modulus of elasticity $E_{frp} = 230,000$ MPa. Fig. 2 shows the meshing of quarter of the concrete circular slice. Two extreme values of d_c are investigated: (i) $d_c = 0$; and (ii) $d_c = 0$ before concrete reaches the unconfined concrete peak stress f'_c, while $d_c = 1 - \sigma_c/f'_c$ for a point on the post-peak stress-strain curve at a stress σ_c. The concrete dilation angle is assigned a value $\psi = 30^\circ$ and the remaining plasticity parameters are assigned the values specified in the "*Plasticity Parameters*" section. As can be seen in Fig. 3(a) and (b), the compressive damage parameter, d_c, has a little effect on the stress-strain curve of FRP-confined concrete and more important effect on the lateral dilation. Given that the damage parameter affects slightly the stress-strain curve, and that only modeling of monotonic loading is considered, the effect of the compressive damage is neglected and $d_c = 0$ is adopted.

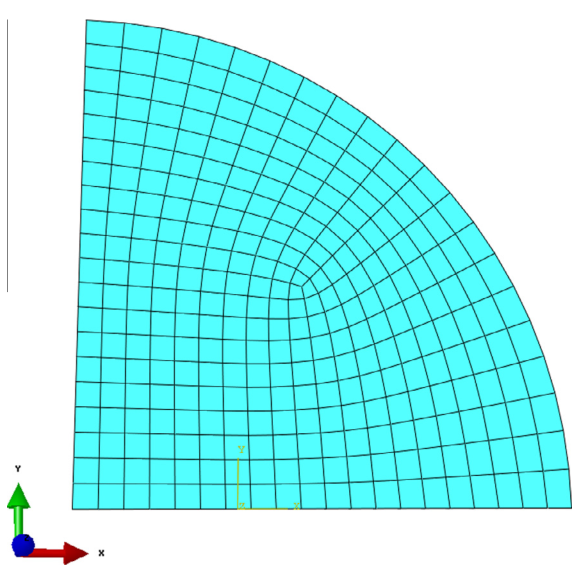

Fig. 2. Meshing of quarter the circular slice.

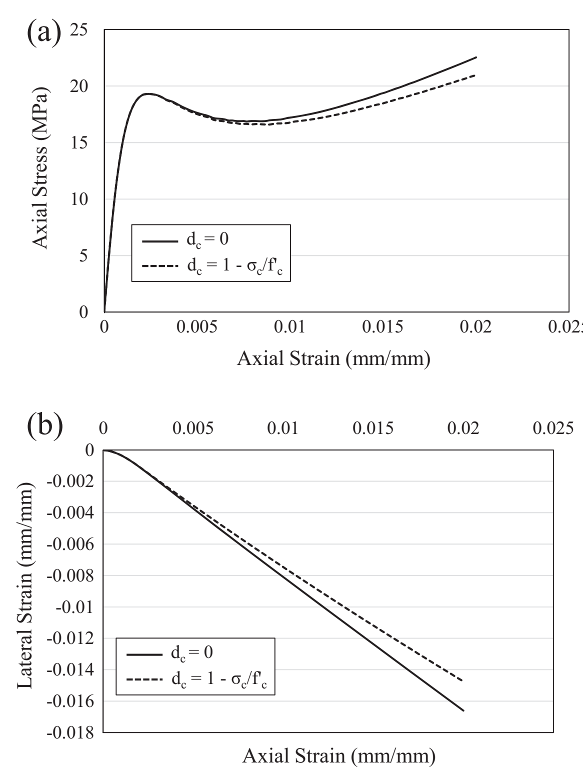

Fig. 3. Influence of d_c on: (a) the stress-strain curve, (b) the lateral strain - axial strain curve of FRP-confined concrete.

3.3.2.3. Plasticity parameters. The remaining parameters needed to model the concrete compressive behavior are designated in the plasticity section of the CDPM, i.e. ψ, f_{bo}/f'_c, K_c, e, and the viscosity parameter.

It has been reported in the literature that the flow potential eccentricity, e, and the viscosity parameter have no important influence on the prediction accuracy [36]. Default value of 0.1 is assigned to e, and a value of 10^{-7} (very close to the default value of zero) is assigned to the viscosity parameter.

Experimental tests are available in the literature to quantify the ratio f_{bo}/f'_c and the following empirical equation is proposed by Papanikolaou and Kappos [39] based on statistical analysis of a large set of test data:

$$\frac{f_{bo}}{f'_c} = 1.5(f'_c)^{-0.075} \tag{8}$$

where f'_c is in MPa.

The parameter K_c controls the shape of the yield surface in the deviatoric plane when the minimum principal effective stress is positive. Consequently, K_c affects the behavior of confined concrete in the case of non-uniform biaxial confinement. However, K_c also defines the yield surface in the different meridian planes. In fact, for positive values of $\hat{\bar{\sigma}}_{\min}$, Eq. (4) reduces to:

$$F = \frac{1}{1-\alpha}(\bar{q} - 3\alpha\bar{p} - \gamma\hat{\bar{\sigma}}_{\min}) - \bar{\sigma}_c(\widetilde{\varepsilon_c^{pl}}) = 0 \tag{9}$$

Different values of γ corresponding to different values of K_c draw different yield surfaces in the meridian planes. In the case of uniformly confined concrete, the 3D loading path is always on the compressive meridian of the failure surface. In this case $\hat{\bar{\sigma}}_{\min}$ is the uniform confining pressure $\hat{\bar{\sigma}}_{\min} = \bar{\sigma}_1 = \bar{\sigma}_2$ and F is expressed as:

$$F = \frac{1}{1-\alpha}(\bar{q} - 3\alpha\bar{p} - \gamma\bar{\sigma}_1) - \bar{\sigma}_c(\widetilde{\varepsilon_c^{pl}}) = 0 \tag{10}$$

which indicates that K_c modifies the yield surface of uniformly confined concrete.

K_c is directly related to f_{bo}/f'_c. According to Yu et al. [11], if the expression proposed by Teng et al. [40] is used to compute the peak stress f'^{*}_{cc} of concrete confined by a constant confining pressure $\sigma_l(f'^{*}_{cc} = f'_c + 3.5\sigma_l)$, K_c reduces to:

$$K_c = \frac{5.5 f_{bo}}{3f'_c + 5f_{bo}} \tag{11}$$

For the unconfined concrete compressive strength $f'_c = 18$ MPa used to perform all the parametric studies, $f_{b0}/f'_c = 1.208$, close to the default value of 1.16, and $K_c = 0.735$. It will be shown when modeling actively-confined concrete, that K_c is responsible for defining the peak stress value of actively-confined concrete.

Using CDPM, the effect of the dilation angle, ψ, is such that an increase in ψ results in an increase in the lateral dilation of concrete confined with FRP and accordingly in the concrete axial stress.

4. Modified concrete damaged plasticity model for FRP-confined concrete

As a result of the parametric studies performed on FRP-confined concrete cylinder, it was found that the dilation angle, ψ, has a significant effect on both the stress-strain curve and lateral strain-axial strain curve. In addition, it is well known that the definition of the compression hardening data dictates the stress-strain curve of FRP-confined concrete modeled using CDPM. Also as Fig 3(a) shows, using the unconfined concrete stress-strain curve to define compression hardening fails to predict the stress-strain curve of FRP-confined concrete. This conclusion was previously made by Yu et al. [11,25], Rousakis et al. [21] and Karabinis and Rousakis [41], who proposed including the confining pressure as a parameter to define the concrete compression hardening. The dilation angle and the damage parameter were also included in the definition of the compression hardening rule in [21,41] where the damage parameter was defined as a function of the concrete strength.

In order to accurately predict the stress-strain curve and the lateral strain-axial strain curve of FRP-confined concrete modeled using CDPM, the compression hardening data and the dilation angle should be well defined.

4.1. Dilation angle

As previously mentioned, the dilation angle is the only parameter that affects the lateral strain-axial strain curve. Defining a constant dilation angle in CDPM results in almost the same lateral strain-axial strain curve for different values of the FRP-jacket stiffness which is inconsistent with experimental observations where the increase in the FRP-jacket stiffness results in a reduction of the lateral dilation. Many plasticity models available in the literature that used a non-associated flow rule to model FRP-confined cylinders assumed a constant potential function parameter or a constant dilation angle [10,15]. Eid and Paultre [13] who proposed a Drucker-Prager type plasticity model for FRP-confined cylinders, expressed the dilatancy angle as a function of the lateral stiffness ratio. Also, Rousakis et al. [21], who analyzed FRP-confined cylinders using a non-associated flow rule in a Drucker-Prager type plasticity model, found that the plastic dilation is dependent on the concrete strength and the jacket confinement modulus. Increasing the confinement modulus or decreasing the concrete strength results in a restriction of the plastic dilation rate. Accordingly, Rousakis et al. [21] proposed closed-form expression of the plastic dilation parameter for low and high strength concrete function of the modulus of confinement and the concrete strength. Yu et al. [25], who used CDPM in ABAQUS [23], related the dilation angle ψ to *the potential function parameter* β by the following expression:

$$\beta = (\sqrt{3}/9)\tan\psi \tag{12}$$

Yu et al. [25] proposed that β, in uniformly-confined sections, is dependent on the plastic deformation $\widetilde{\varepsilon_p}$, the confining pressure σ_l, and the rate of confinement increment. Accordingly, defining the dilation angle ψ of FRP-confined concrete requires obtaining a series of lateral strain-axial strain $(\varepsilon_l - \varepsilon_c)$ relationships for different $E_{frp}t_{frp}/R$, and computing β and ψ as a function of the equivalent plastic strain. The following equation, proposed by Teng et al. [40], was used by Yu et al. [25] to generate the lateral strain-axial strain curves:

$$\phi\left(\frac{-\varepsilon_l}{\varepsilon_{co}}\right) = \frac{\varepsilon_c}{\varepsilon_{co}} \bigg/ \left(1 + 8\frac{\sigma_l}{f'_c}\right) = 0.85\left\{\left[1 + 0.75\left(\frac{-\varepsilon_l}{\varepsilon_{co}}\right)\right]^{0.7} - \exp\left[-7\left(\frac{-\varepsilon_l}{\varepsilon_{co}}\right)\right]\right\} \tag{13}$$

where $\sigma_l = -K_l\varepsilon_l$.

It should be noted that Lim and Ozbakkaloglu [42] found that Eq. (13) represented one of the best performing models in predicting the lateral strain-axial strain curves of concrete specimens of circular cross-section of normal and high strength confined with FRP. Accordingly, this expression is adopted to derive the dilation angle model explained hereafter.

In the following, calibration of the dilation angle to predict the theoretical lateral strain-axial strain curve of FRP-confined concrete is performed. For FRP-confined circular specimens, the lateral strain-axial strain curve depends on the ratio of the stiffness of the FRP jacket, K_l, to the unconfined concrete compressive strength, f'_c, K_l/f'_c where $K_l = E_{frp}t_{frp}/R$. To calibrate the dilation angle of FRP-confined circular specimens, theoretical curves proposed by Teng et al. [40] (Eq. (13)) are first generated for different values of K_l/f'_c ranging from 0 to 40 as shown in Fig. 4(a) and (b). As can be seen in these figures, beyond an axial strain close to 0.002 the lateral strain-axial strain curve becomes almost linear, and therefore, in FE modeling, a constant dilation angle is proposed for each value of K_l/f'_c. Finite Element simulations are then performed on the same circular specimen used in the parametric evaluation, and the FRP-jacket thickness, t_{frp}, is varied to achieve the values of K_l/f'_c shown in Table 1. For each value of the FRP-jacket thickness, t_{frp}, i.e. for each value of K_l/f'_c, a value of the dilation angle ψ is specified in ABAQUS [23] such that the lateral strain-axial strain curve obtained in FE simulation matches approximately the theoretical lateral strain-axial strain curve given by Eq. (13) as can be seen in Fig. 4(a) and (b). Table 1 shows, for each K_l/f'_c the dilation angle ψ specified in ABAQUS [23] to predict the corresponding theoretical axial strain-lateral strain curve. As can be seen in Table 1, to the value $K_l/f'_c = 40$ corresponds the minimum dilation angle allowed in ABAQUS [23] ($\psi = 0.1°$, very close to zero) and beyond this value the theoretical lateral dilation cannot be predicted accurately using CDPM. The plot in Fig. 5 shows that a linear relationship exists between ψ and K_l/f'_c (presented in Table 1), which can be expressed as follows:

$$\psi = -1.4587\frac{K_l}{f'_c} + 57.296 \quad \text{for } 0 \leqslant \frac{K_l}{f'_c} \leqslant 40 \tag{14}$$

As stated previously, the lateral dilation of FRP-confined circular specimens cannot be predicted in ABAQUS [23] for $K_l/f'_c > 40$, and therefore the proposed dilation angle expression (Eq. (14)) is limited for values of K_l/f'_c ranging between zero and 40. According to Eq. (14), for K_l/f'_c close to zero and 40 respectively, ψ is slightly greater than 56 and lower than 0.1, in which case ψ values greater than 56 or lower than 0.1 will be substituted by 56 and 0.1, respectively. Eq. (14) does not consider the variation of the dilation angle as a function of the equivalent plastic strain as Yu et al. [25] proposed. However, as shown in Fig. 4(a) and (b), assuming the dilation angle to be dependent only on K_l/f'_c leads to close predictions of the theoretical curves while adopting a simple procedure.

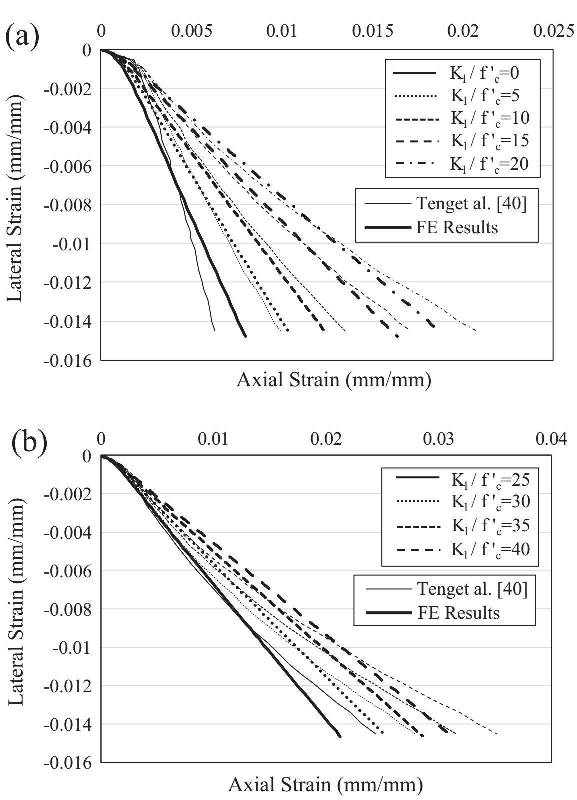

Fig. 4. Theoretical versus FE lateral strain-axial strain curves for: (a) $0 \leqslant K_l/f'_c \leqslant 20$, (b) $25 \leqslant K_l/f'_c \leqslant 40$.

Table 1
Variation of the dilation angle, ψ, with respect to the ratio of the stiffness of the FRP-jacket to the unconfined concrete compressive strength, K_l/f'_c.

K_l/f'_c	0	5	10	15	20	25	30	35	40
ψ	56	50	45	35	28	22	12	5	0.1

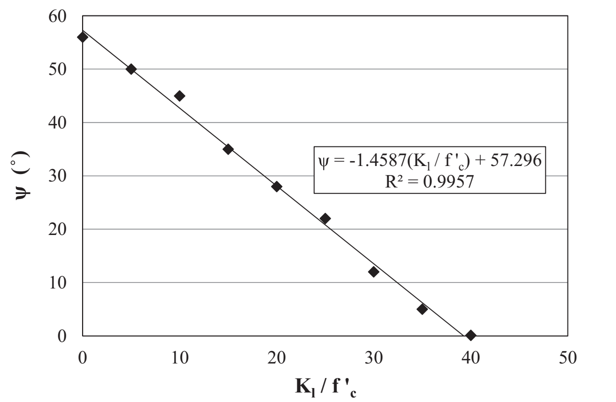

Fig. 5. Regression analysis of the dilation angle, ψ, with respect to the ratio of the stiffness of the FRP-jacket to the unconfined concrete compressive strength, K_l/f'_c.

For specimens of square or rectangular cross-section or for partially wrapped specimens, the definition of the dilation angle is complex due to the non-uniformity of the lateral dilation. Two methods are proposed to define the dilation angle in this case:

4.1.1. Method I

Define a constant dilation angle for the whole concrete volume by substituting K_l/f'_c in Eq. (14) by $(A_e/A_c)(K_l/f'_c)$ where A_e/A_c is the confinement effectiveness coefficient representing the ratio of the effectively confined area A_e, to the cross section area A_c. For fully confined plain square or rectangular columns, Fig. 6 shows the area of the cross-section effectively confined, and the parameter A_e/A_c is expressed as:

$$\frac{A_e}{A_c} = 1 - \frac{(b/h)(h-2r)^2 + (h/b)(b-2r)^2}{3A_c} \tag{15}$$

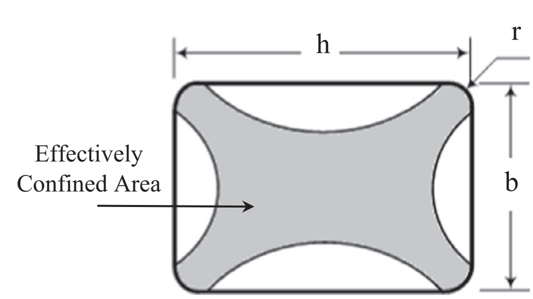

Fig. 6. Effectively confined area of a rectangular cross-section.

where b and h are the dimensions of the square or rectangular cross-section, r is the corner radius.

For fully confined circular columns, $A_e/A_c = 1.0$. For partially confined circular or rectangular columns, the confinement effectiveness coefficient A_e/A_c should be multiplied by a coefficient k_v given by the following equations [38]:

$$k_v = \left(1 - \frac{s'}{2D}\right)^2 \quad \text{for circular columns} \tag{16}$$

where D is the diameter of the circular section and s' is the clear spacing of the transverse FRP strips (Fig. 7).

$$k_v = \left(1 - \frac{s'}{2b}\right)\left(1 - \frac{s'}{2h}\right) \quad \text{for rectangular columns} \tag{17}$$

For square or rectangular cross-sections, the equivalent radius defined as $R = \sqrt{b^2 + h^2}/2$ is used to compute K_l.

4.1.2. Method II

This method utilizes the fact that for a concrete column of circular section fully confined by FRP, $K_l = E_{frp}t_{frp}/R = -\sigma_l/\varepsilon_l$. The expression given in Eq. (14) can be used to define the dilation angle of each element of the concrete as a function of the equivalent confining pressure σ_l acting on the element, and its lateral dilation ε_l. The equivalent confining pressure is defined according to Yu et al. [25] as:

$$\sigma_l = \frac{2(\sigma_2 + 0.039f'_c)(\sigma_3 + 0.039f'_c)}{(\sigma_2 + \sigma_3 + 0.078f'_c)} - 0.039f'_c \tag{18}$$

where σ_2 and σ_3 are the two principal lateral stresses respectively, and ε_l is the average lateral strain defined as:

$$\varepsilon_l = \frac{\varepsilon_2 + \varepsilon_3}{2} \tag{19}$$

where ε_2 and ε_3 are the two principal lateral strains.

For non-circular cross-sections, Yu et al. [25] used this same procedure to define the rate of confinement increment needed as a parameter to evaluate ψ in their model along with the equivalent plastic strain and the confining pressure.

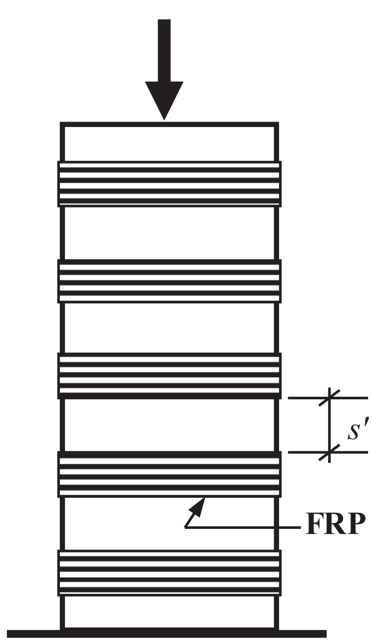

Fig. 7. Configuration of partially wrapped specimens.

According to *Method II*, the dilation angle ψ of each element is defined as a function of the effective confining pressure σ_l and the lateral strain ε_l that vary during the analysis. ABAQUS [23] allows the material properties (dilation angle and compression hardening) to be modified progressively with variation in the field variables during the solution process. The field variable associated with the dilation angle is defined in the user subroutine *USDFLD* coded in FORTRAN as the ratio of the effective confining pressure σ_l (Eq. (18)) to the negative of the average lateral strain ε_l (Eq. (19)), $(-\sigma_l/\varepsilon_l)$. Calling this subroutine requires including the **USER DEFINED FIELD* option in the definition of the concrete material. Results of both methods (*Methods I and II*) are shown when comparing the proposed model versus experimental results discussed in a subsequent section of this paper.

4.2. Hardening/softening rule

It is well known that, for FRP-confined concrete columns, the confining pressure provided to the concrete core is not constant during loading but increases as concrete dilation increases. It has been widely stated in the literature that the stress-strain curve of FRP-confined concrete can be constructed as a set of points on a series of curves of actively-confined concrete, as shown in Fig. 8. Accordingly, many analysis-oriented models were proposed based on this principle [40,43–45]. At the intersection points between the FRP-confined concrete stress-strain curve and the series of stress-strain curves of actively-confined concrete, i.e. for a given axial strain, both the FRP-confined concrete and the actively-confined concrete have the same confining pressure and lateral strain.

A recent experimental investigation performed by Lim and Ozbakkaloglu [46] assessed the assumption of stress path independency for normal strength concrete (NSC), and high strength concrete (HSC). This examination showed that for NSC, at a given axial and lateral strain and confining pressure, a slightly lower stress is exhibited by FRP-confined concrete as compared to actively-confined concrete. The difference between the two curves is more important for HSC and it grows larger as the concrete strength increases. In return, the assumption of path independency was approved for the lateral strain-axial strain relationship [46] given that this relationship was found only dependent on the instantaneous confining pressure and not on the application path for both NSC and HSC. Based on their findings, Lim and Ozbakkaloglu proposed a unified stress-strain model for FRP and actively confined concrete of both normal and high strength [47]. With the aim of assessing the difference in the axial stresses ($\Delta\sigma_c$) previously described, Lim and Ozbakkaloglu [47] computed experimentally the difference in the confining pressures $\Delta\sigma_l$ between the two companion specimens at a given axial strain ε_c and stress

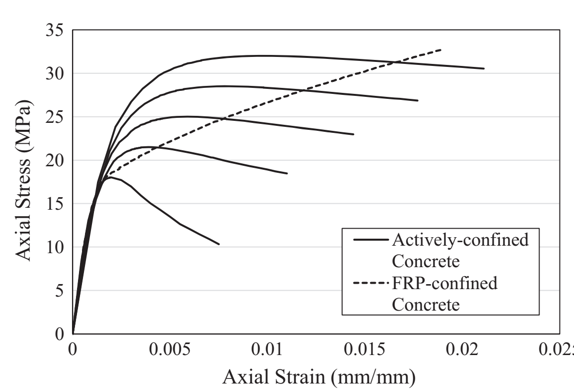

Fig. 8. Typical stress-strain curves of actively-confined concrete and FRP-confined concrete.

σ_c. Using regression analysis, the following expression of $\Delta\sigma_l$ was proposed [47]:

$$\Delta\sigma_l = 0.13 f_c'^{0.24} K_l^{0.95} \varepsilon_l \tag{20}$$

where $\Delta\sigma_l$, f_c' and K_l are expressed in MPa.

Accordingly, Lim and Ozbakkaloglu [47] proposed a model to generate the axial stress-strain and lateral strain-axial strain curves that follows an incremental procedure similar to that suggested by Teng et al. [40] (presented later in this paper) yet considering different constitutive expressions. The major difference between the two models is that according to Teng et al. [40], at a given lateral strain, the lateral confining pressure σ_l that is computed depending on the stiffness of the FRP jacket, is used to define the axial strain and stress. As for Lim and Ozbakkaloglu [47], σ_l is used to compute the axial strain at a given lateral strain, whereas, whereas $\sigma_l^* = \sigma_l - \Delta\sigma_l$ is considered when determining the axial stress; $\Delta\sigma_l$ is defined according to Eq. (20).

Yu et al. [25] used the assumption of path independency of both the stress and the lateral strain–axial strain relationship to define the *compression hardening data*, the *damage parameter* and the *dilation angle* of FRP-confined concrete. The dilation angle definition of Yu et al. [25] was previously explained. According to Yu et al. [25], at a given confining pressure and plastic strain, the compression hardening data and the damage data correspond to the data of actively-confined concrete at the same confining pressure and plastic strain. Therefore, the hardening/softening rule of FRP-confined concrete was made dependent on the confining pressure defined as a field variable. For each confining pressure, the compression hardening data was found using the theoretical stress-strain curve proposed by Teng et al. [40] for actively confined concrete.

In this study, as mentioned earlier, a zero damage variable is considered to model FRP-confined concrete subject to monotonic loading.

As for the compression hardening data of FRP-confined concrete, the current study adopts Yu et al. [25] concept with modification of the definition of the hardening/softening rule for actively-confined concrete and with incorporation of the new findings of Lim and Ozbakkaloglu [47] related to the path independency and described previously. The new hardening/softening rule will be presented in the following. In order to account for the findings of Lim and Ozbakkaloglu [47], the confining pressure (used as the first field variable) is defined as $\sigma_l' = \sigma_l - \Delta\sigma_l$ where σ_l is the confining pressure computed based on the actual lateral stresses (Eq. (18)) and $\Delta\sigma_l$ (Eq. (20)) defines the reduction of lateral stress in FRP-confined concrete relative to actively-confined concrete. For circular specimens, the terms K_l and ε_l in Eq. (20) are defined respectively as $E_{frp}t_{frp}/R$ and $(\varepsilon_2 + \varepsilon_3)/2$ (Eq. (19)). For square and rectangular specimens, ε_l is also defined according to Eq. (19) whereas two methods are used to define K_l similar to Methods I and II used to define the dilation angle and described previously. It should be noted that σ_l used to define K_l according to method II ($K_l = -\sigma_l/\varepsilon_l$), is defined as by Eq. (18) without subtracting $\Delta\sigma_l$ given that the assumption of path independency was found valid for defining the lateral strain.

A new strain hardening/softening rule is proposed to predict the stress-strain curve of actively-confined concrete for different confining pressures. A parametric study is performed on actively-confined concrete to investigate the sensitivity of the stress-strain response to variations in the input material parameters and for calibrating the input compression hardening data.

4.2.1. Parametric study for actively-confined concrete

For actively confined concrete, the parametric study is performed on the same circular specimen of radius $R = 100$ mm, compressive strength $f_c' = 18$ MPa and corresponding axial strain $\varepsilon_{co} = 0.002$ with an applied constant confining pressure, $\sigma_l = 5$ MPa. The first loading step defined in ABAQUS [23] corresponds to the application of the confining pressure and in the second step a prescribed displacement is applied to simulate the vertical loading. The two parameters whose effect on the stress-strain curve is evaluated through parametric study are K_c and ψ. To perform the parametric studies, Popovics [37] is used to generate the compression hardening data.

For an unconfined concrete compressive strength $f_c' = 18$ MPa, K_c was previously found equal to 0.735. Seow and Swaddiwudhipong [48] reported that experimental values of K_c range between 0.5 and 1. An investigation on the effect of K_c on the stress-strain curve is shown in Fig. 9 where values of 0.6, 2/3 (default value in ABAQUS [23]), 0.735 (Eq. (11)) and the upper limit 1 are considered. Values of K_c lower than 0.6 are not considered in the study since the definition of the yield surface in ABAQUS [23] includes $\gamma = 3(1-K_c)/(2K_c-1)$ and therefore values close to 0.5 make the denominator close to zero. To perform the parametric study, the dilation angle of concrete is assigned a value $\psi = 30^\circ$ and the remaining plasticity parameters are assigned the values as explained previously in the "*Plasticity Parameters*" section. As can be seen in Fig. 9, K_c controls the magnitude of peak stress of confined concrete where higher values of K_c lead to smaller peak stress. Fig. 9 plots also the analysis oriented model, initially proposed by Mander et al. [38], with modifications of the peak compressive strength expression proposed by Teng et al. [40] and expressed as follows:

$$\frac{\sigma_c}{f_{cc}'^*} = \frac{(\varepsilon_c/\varepsilon_{cc}^*)r}{r - 1 + (\varepsilon_c/\varepsilon_{cc}^*)^r} \tag{21}$$

where $(\varepsilon_c, \sigma_c)$ are the coordinates of a point on the stress-strain curve of actively confined concrete, $(\varepsilon_{cc}^*, f_{cc}'^*)$ are the coordinates of the peak point of the same curve and r is defined as:

$$r = \frac{E_c}{E_c - \frac{f_{cc}'^*}{\varepsilon_{cc}^*}} \tag{22}$$

$f_{cc}'^*$ and ε_{cc}^* are defined respectively as:

$$\frac{f_{cc}'^*}{f_{co}'} = 1 + 3.5\frac{\sigma_l}{f_{co}'} \tag{23}$$

$$\frac{\varepsilon_{cc}^*}{\varepsilon_{co}} = 1 + 17.5\frac{\sigma_l}{f_{co}'} \tag{24}$$

It should be noted that many analysis oriented stress-strain models have been proposed in the literature and many expressions have been developed to quantify $(\varepsilon_{cc}^*, f_{cc}'^*)$. Lim and Ozbakkaloglu [49]

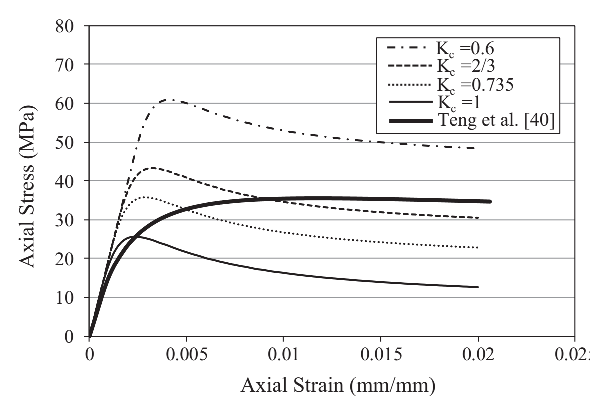

Fig. 9. Influence of K_c on the stress-strain curve of actively-confined concrete.

assessed the performance of all available models of $(\varepsilon^{*}_{cc}, f'^{*}_{cc})$ and found that the expressions of Teng et al. [40] (Eqs. (23) and (24)) performed well in predicting the experimental results. Accordingly, these expressions are adopted in the current study.

It can be seen in Fig. 9 that for $K_c = 0.735$ the peak stress of concrete obtained from FE analysis corresponds to the analytical peak stress obtained from Teng et al. [40].

The sensitivity analysis shows also that the dilation angle ψ has no noticeable effect on the stress-strain curve of actively-confined concrete.

Fig. 10 plots the stress-strain response of circular concrete slices confined with different constant confining pressures with Popovics [37] used to define compression hardening data and the other parameters defined as previously described. As can be seen in Fig. 10, although these curves predict correctly the peak stress of confined concrete, they do not predict accurately the increase of the axial strain at peak stress and the reduction of the steepness of the post-peak branch due to the confining pressure. Therefore, the input compression hardening data must be modified for more accurate prediction of the behavior of actively-confined concrete. Note that using the hardening/softening rule proposed by Yu et al. [25] led to axial stress-strain curves that overestimate the corresponding experimental curves for some of the specimens presented in this paper especially specimens exhibiting a post-peak descending behavior.

4.2.2. Modified strain hardening/softening rule for actively-confined concrete

For each confining stress, the input compression hardening data in ABAQUS [23] is calibrated such that the FE stress-strain curve matches the theoretical stress-strain curve generated by Teng et al. [40] (Eqs. (21)–(24)). The following procedure is adopted, for each value of the confining pressure σ_l:

- The theoretical stress-strain curve is generated using Eqs. (21)–(24).
- The first branch of the unconfined concrete stress-strain curve proposed by Popovics [37] is modified to make the unconfined concrete peak stress occur at a strain ε^{*}_{cc} instead of ε_{co}. This is achieved by computing ε^{*}_{cc} and adding the difference $\varepsilon^{*}_{cc} - \varepsilon_{co}$ linearly to the strain values between 0 and ε_{co} as shown in Fig. 11.
- The post-peak branch of unconfined concrete stress-strain curve [37] is substituted by the theoretical post-peak branch obtained using Teng et al. [40] in which all the stresses values are reduced by $f'^{*}_{cc} - f'_c$ as shown in Fig. 11.

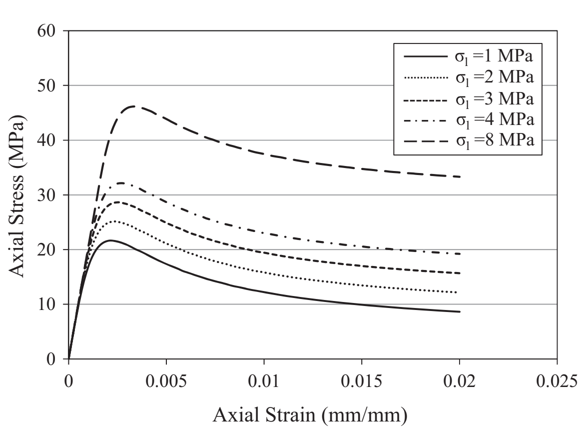

Fig. 10. Stress-strain curves of actively-confined concrete with compression hardening data according to Popovics [37].

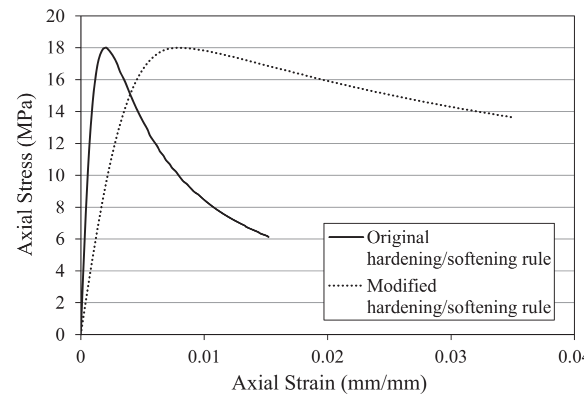

Fig. 11. Original and modified strain/hardening softening rule.

This modified stress-strain curve is used to generate the input compression hardening data. It should be noted that Tao et al. [36] also proposed modifying the input stress-strain curve of unconfined concrete to capture the behavior of concrete filled steel stubs, however the method proposed to modify the curve is slightly different than that used in this study. Fig. 12(a–c) shows that the stress-strain curves obtained from FE analysis using the new compression hardening data compare well with the theoretical model proposed by Teng et al. [40] obtained for σ_l varying from 1 to 9 MPa, i.e. for $\sigma_l/f'_c \leqslant 0.5$. To assess the accuracy of the proposed method for $\sigma_l/f'_c > 0.5$, comparison is made in Fig. 13 between the theoretical stress-strain curves of Teng et al. [40] for $\sigma_l = 10$ MPa and the FE analysis results. The results of FE analysis in Fig. 15 were obtained using two approaches: "FE-Results-*i*" in which the new proposed hardening/softening rule is adopted, and "FE-Results-*ii*" in which Popovics [37] is used to generate the compression hardening data before the peak stress while a perfectly plastic behavior is assumed after the peak stress. It can be seen in Fig. 13 that the results obtained using the two methods are reasonably close. Consequently, for the purpose of simplification, for high confining pressures $(\sigma_l/f'_c > 0.5)$, the hardening/softening rule is modeled using Popovics [37] before the peak stress and a perfectly-plastic behavior after the peak stress.

5. Proposed model versus experimental results

The performance of the proposed model using the modified CDPM for the FRP-confined concrete specimens having different cross-section shapes is validated against experimental results available in the literature. For circular specimens, since *Method I* and *Method II* for defining the dilation angle produce almost similar results for both the stress-strain and the axial strain-lateral strain curves, the results of only *Method I* are reported. For square or rectangular specimens and for partially wrapped specimens, the results of both methods (*Methods I and II*) are reported. It is worth noting that using the concept of field variable to define the input material properties might generate numerical errors. As the confining pressure increases, the hardening/softening curve is modified. In the case where the slope of the new curve is higher than the slope of the previous curve, the lateral strain generated at this step may be lower as well as the new computed confining pressure. This may create numerical errors. To address this problem, an additional condition is imposed on the first field variable in the user subroutine to prevent it from decreasing which is in accordance with the real behavior.

Figs. 14–17 show comparisons of the FE predictions with the test results of Yu et al. [25], Lam and Teng [50], Valdmanis et al.

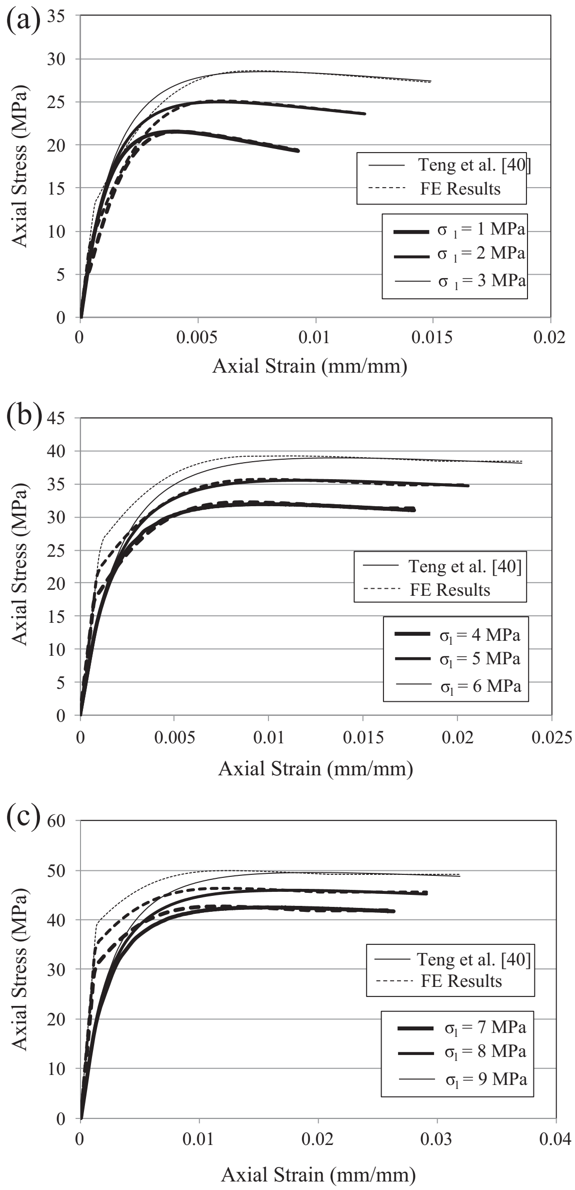

Fig. 12. FE results of actively-confined concrete using modified strain hardening/softening rule versus theoretical results for $\sigma_l/f'_c \leqslant 0.5$.

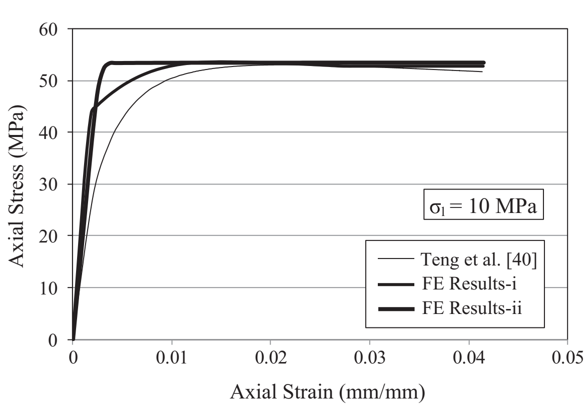

Fig. 13. Comparison between Teng et al. [40] theoretical stress-strain curve for actively-confined concrete with $\sigma_l = 10$ MPa and the FE results using methods *i* and *ii*.

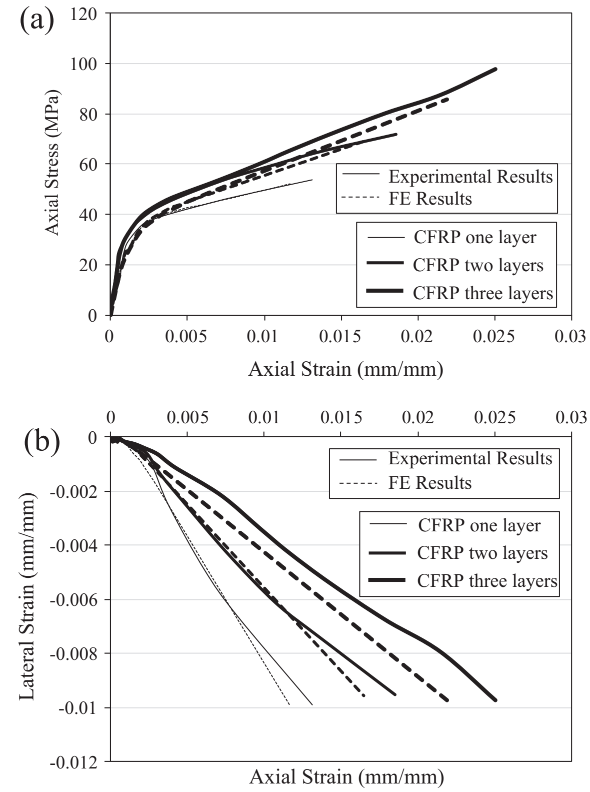

Fig. 14. FE Results versus experimental results of: (a) stress-strain curves and (b) lateral strain-axial strain curves of specimens tested by Lam and Teng [50].

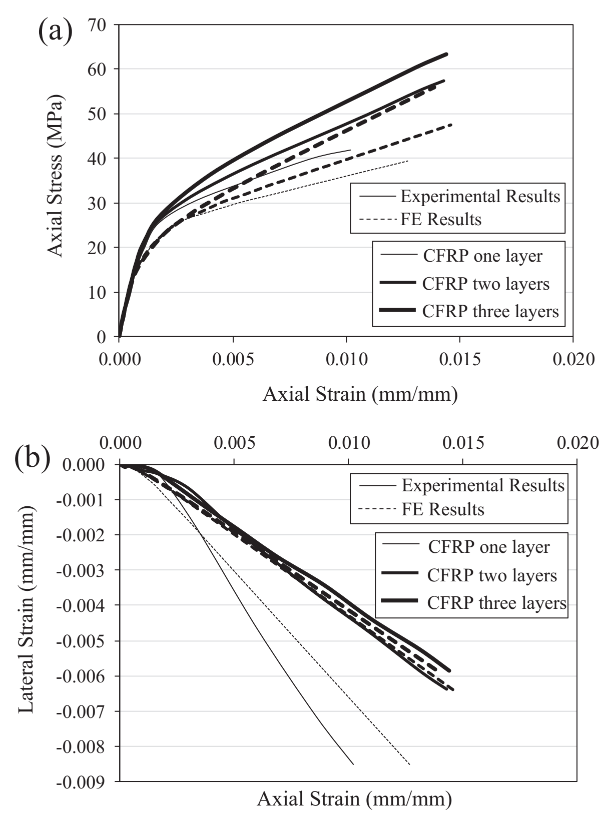

Fig. 15. FE Results versus experimental results of: (a) stress-strain curves and (b) lateral strain-axial strain curves of specimens tested by Valdmanis et al. [51].

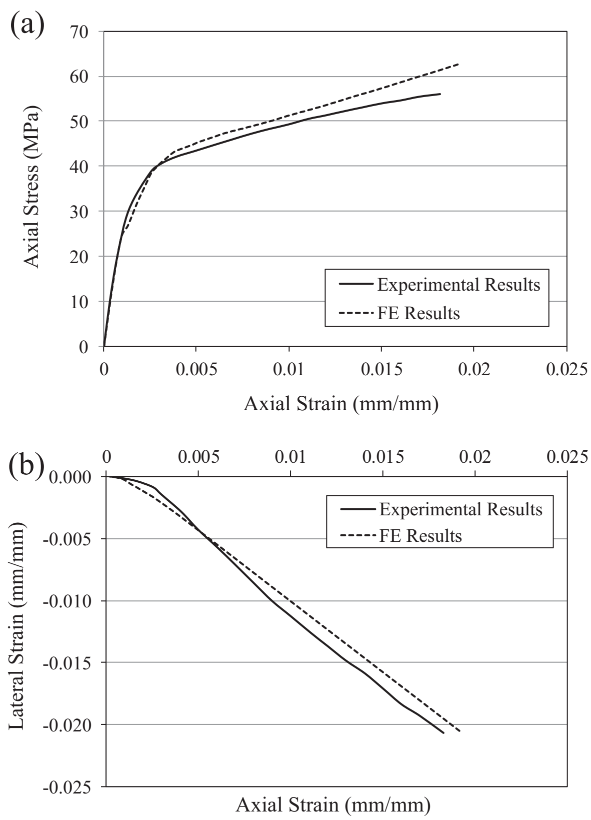

Fig. 16. FE Results versus experimental results of: (a) stress-strain curves and (b) lateral strain-axial strain curves of specimens tested by Wong et al. [52].

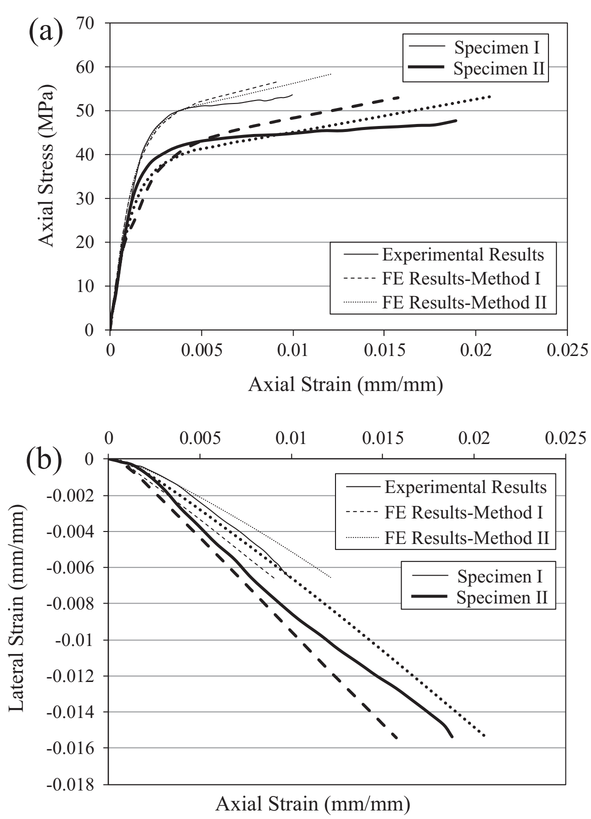

Fig. 17. FE Results versus experimental results of: (a) stress-strain curves and (b) average corner hoop strain-axial strain curves of specimens reported by Yu et al. [25].

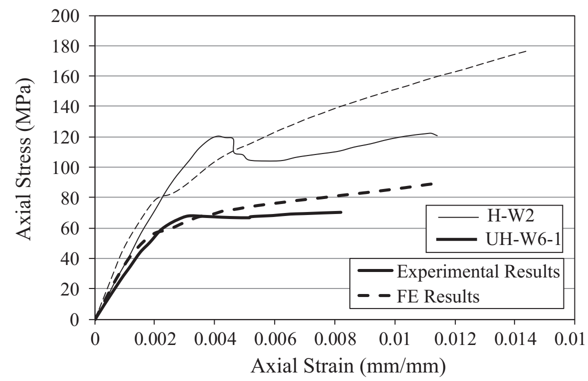

Fig. 18. Comparison between the experimental and FE stress-strain curves of specimens UH-W6-1 and H-W2 tested by Vincent and Ozbakkaloglu [53].

[51], and Wong et al. [52]. Comparisons are shown for both the stress-strain response and the lateral strain-axial strain response, respectively. The FE results are also compared in Figs. 18–20 with the test data of FRP confined specimens reported recently by Vincent and Ozbakkaloglu [53], Ozbakkaloglu [54,55] and Hany et al. [9]. The details of all the specimens are provided in Table 2. The experimental curves of *H-W2*, *A20R15L5* and *A10R30L5* are obtained as the average of many identical specimens tested. All the specimens are fully wrapped over their entire height except specimens *CP1*, *SP1*, *R1P1* and *R2P1* that are wrapped with discontinuous FRP strips of width $W = 50$ mm and spaced at $s' = 50$ mm (Fig. 7). All the specimens are wrapped with CFRP sheets except the specimens of Ozbakkaloglu [54,55] and Wong et al. [52] that are confined with an FRP tube. In Table 2, H is the specimen height and ε_{co} is the strain at the unconfined concrete strength. For the specimens tested by Lam and Teng [50], a value of $\varepsilon_{co} = 0.002$ is assumed given that the exact value was not reported. Lam and

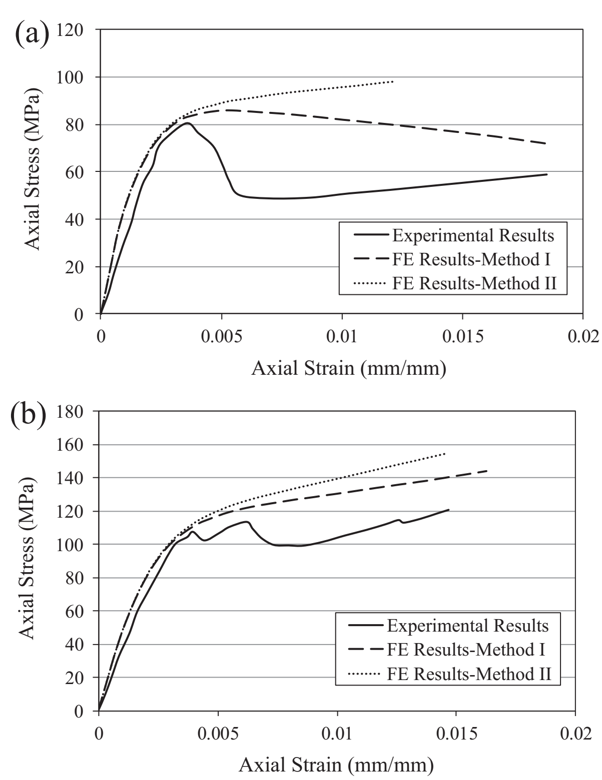

Fig. 19. Comparison between the experimental and FE stress-strain curves of specimens (a) *A20R15L5* [54] and (b) *A10R30L5* [55].

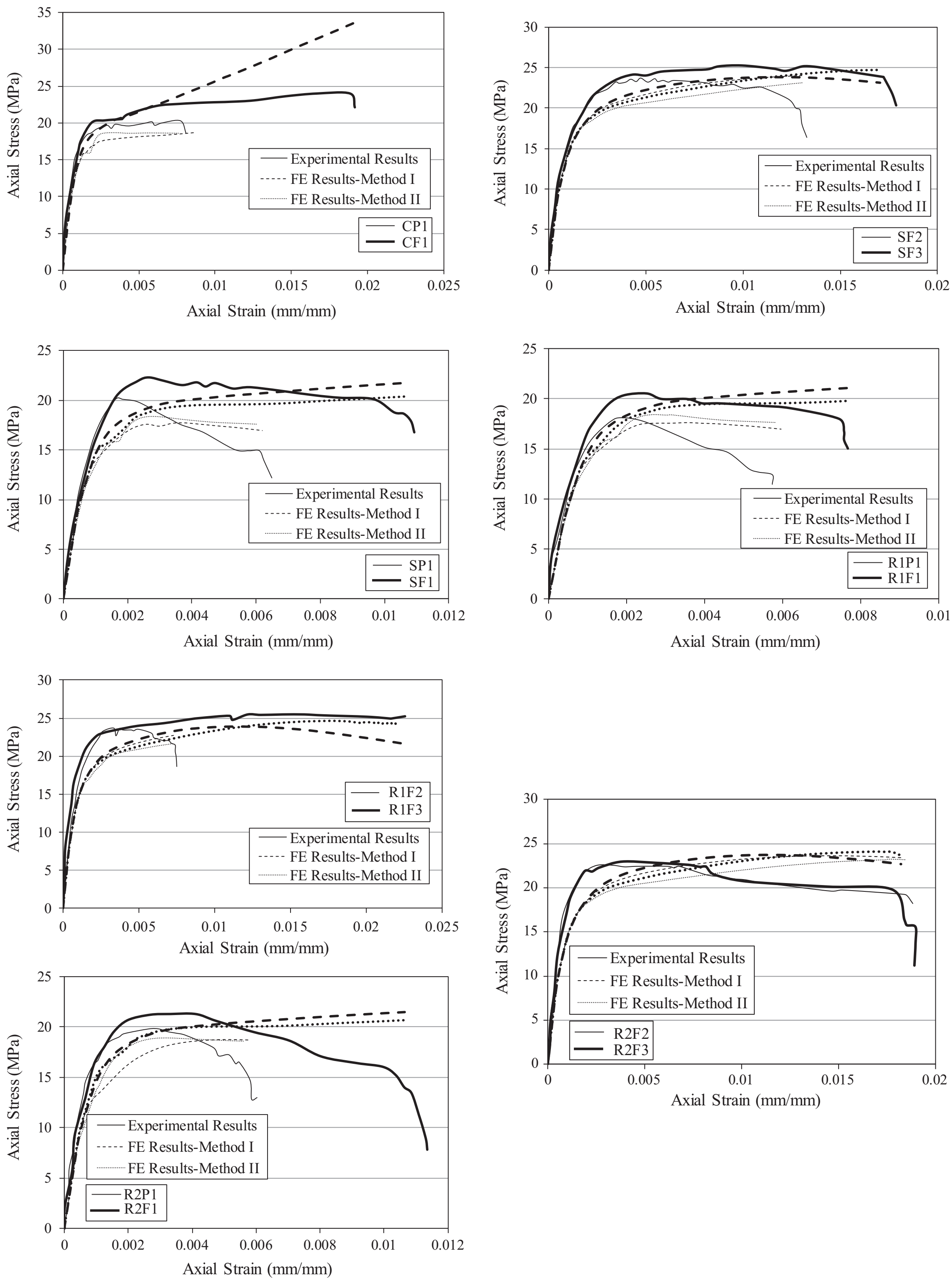

Fig. 20. FE Results versus experimental results of stress-strain curves of specimens tested by Hany et al. [9].

Teng [50] reported an initial modulus of elasticity of concrete $E_c = 27,981$ MPa for the specimens wrapped with one and two layers of CFRP and a modulus of $E_c = 29,828$ MPa for the specimen wrapped with three layers. Valdmanis et al. [51] reported $E_c = 24,400$ MPa for all the three specimens. For the remaining specimens, E_c is computed as $E_c = 4730\sqrt{f'_{co}}$. Note that in Figs. 14–19, the curves are terminated at a lateral strain corresponding to the experimental hoop rupture strain. For the specimens of Hany et al. [9], since the experimental lateral strains were not reported

Table 2
Summary of specimens' details.

Paper	Specimen	Cross-section	D (mm)	b (mm)	h (mm)	r (mm)	H (mm)	f'_c (MPa)	ε_{co} (mm/mm)	E_{frp} (MPa)	t_{frp} (mm)
Lam and Teng [50]	CFRP one layer	Circle	152	–	–	–	305	35.9	0.0020	230,000	0.165
	CFRP two layers										0.330
	CFRP three layers							34.3			0.495
Valdmanis et al. [51]	CFRP one layer	Circle	150	–	–	–	300	23.3	0.0020	234,000	0.170
	CFRP two layers										0.340
	CFRP three layers										0.510
Wong et al. [52]	–	Circle	152	–	–	–	305	39.6	0.0026	80,100	0.340
Yu et al. [25]	Specimen I	Square	–	150	150	24.0	–	46.0	0.0026	250,000	0.330
	Specimen II					25.0		37.5	0.0031	80,100	0.510
Vincent and Ozbakkaloglu [53]	H-W2	Circle	152	–	–	–	305	64.5	0.0027	240,000	0.234
	UH-W6-1	Circle	152	–	–	–	305	110.0	0.0035	240,000	0.702
Ozbakkaloglu [54]	A20R15L5	Rectangle	–	112.5	225	15.0	300	78.2	0.0030	240,000	1.170
Ozbakkaloglu [55]	A10R30L5	Square	–	150	150	30.0	300	107.3	0.0035	240,000	1.170
Hany et al. [9]	CP1	Circle	200	–	–	–	500	18.0	0.0020	230,000	0.130
	CF1										0.130
	SP1	Square	–	160	160	10.0	500				0.130
	SF1										0.130
	SF2										0.260
	SF3										0.390
	R1P1	Rectangle	–	140	180	10.0	500				0.130
	R1F1										0.130
	R1F2										0.260
	R1F3										0.390
	R2P1	Rectangle	–	130	200	10.0	500				0.130
	R2F1										0.130
	R2F2										0.260
	R2F3										0.390

due to the large scatter in the measured values, the analytically predicted stress-strain curves were terminated at the axial strains corresponding to a sudden drop in the experimental stress-strain response.

It can be seen from Figs. 14–20 that the FE results obtained using the proposed modified CDPM model are in close agreement with test results reported in the technical literature. It can also be seen for the two square specimens in Fig. 17(a), and for the square, rectangular and partially wrapped specimens in Fig. 20 that both methods (*Methods I and II*) lead to good predictions of the experimental stress-strain curves. However, as can be seen in Fig. 17(b), for the average corner hoop strain-axial strain curves, at the same axial strain, lower corner hoop strain is obtained using *Method II* when compared to *Method I*. This is attributed to the fact that using Method II, the dilation angle in the corner region where the confining pressures are high is lower than the constant value specified using Method I. For the HSC circular specimen, *H-W2* (Fig. 18), and the UHSC square specimen *A10R30L5* (Fig 19b) close agreement is observed between the experimental and FE results. The discrepancy between the experimental and FE results increases for circular specimens of higher concrete strengths (*Specimen UH-W6-1* in Fig. 19). As for specimen *A20R15L5*, it can be seen that using *Method I* allows a good representation of the experimental results. However, *Method II* overestimates the stress in the specimen and the high dilation angle in the region close to the flat sides causes the lateral strain to reach the experimental rupture value early.

6. Summary and conclusions

In this paper, concrete damaged plasticity model available in ABAQUS software is used to simulate concrete columns confined with FRP jackets when subjected to monotonic axial compressive loading. A parametric study was carried out to evaluate the sensitivity of the stress-strain and lateral strain-axial strain responses to different input materials parameters. Based on the results of this study, modifications were introduced to the concrete damaged plasticity model (CDPM) used in ABAQUS for FE modeling of FRP-confined concrete columns under monotonically applied axial compression.

For columns of circular cross-section, a new hardening/softening rule is proposed to predict the stress-strain behavior of concrete with different active (or constant) confining pressures. For FRP-confined concrete, a new expression of the dilation angle is generated and the compression hardening/softening rule is defined as a function of the confining pressure that varies during loading. The actual confining pressure is reduced by a specified amount that takes into account the path dependency of the concrete stress and is defined as a field variable using the user subroutine USDFLD available in ABAQUS.

For FRP-confined specimens of non-circular cross-section (i.e. square or rectangular) or specimens wrapped with discontinuous strips, the definition of the compression hardening/softening rule is similar to circular specimens. However, in this case, two methods are proposed to define the dilation angle and lead to close predictions for normal strength concrete and larger difference for higher concrete strengths.

The results of the proposed modified CDPM were compared with experimental results of FRP-confined circular and rectangular concrete specimens reported in the literature. FE results generated using the proposed model were in very good agreement with the test data.

Acknowledgments

This research is supported by the Lebanese National Council for Scientific Research. The authors are most grateful for that support, and for the Faculty of Engineering and Architecture at AUB for providing the computer facilities.

References

[1] Ozbakkaloglu T, Lim JC, Vincent T. FRP-confined concrete in circular sections: Review and assessment of stress-strain models. Eng Struct 2013;49:1068–88.
[2] Lim JC, Ozbakkaloglu T. Design model for FRP-confined normal- and high-strength concrete square and rectangular columns. Mag Concr Res 2014;66 (20):1020–35.
[3] Fahmy MFM, Wu Z. Evaluating and proposing models of circular concrete columns confined with different FRP composites. Composites B 2010;41 (3):199–213.
[4] Nisticò N, Pallini F, Rousakis T, Wu YF, Karabinis A. Peak strength and ultimate strain prediction for FRP confined square and circular concrete sections. Composites B 2014;67:543–54.
[5] De Lorenzis L, Tepfers R. Comparative study of models on confinement of concrete cylinders with fiber-reinforced polymer composites. J Compos Constr, ASCE 2003;7(3):219–34.
[6] Lam L, Teng JG. Stress-strain model for FRP-confined concrete under cyclic axial compression. Eng Struct 2009;31(2):308–21.
[7] Wang Z, Wang D, Smith S, Lu D. CFRP-confined square RC columns. II: Cyclic axial compression stress-strain model. J Compos Constr, ASCE 2012;16 (2):161–70.
[8] Wang Z, Wang D, Smith S, Lu D. Experimental testing and analytical modeling of CFRP-confined large circular RC columns subjected to cyclic axial compression. Eng Struct 2012;40:64–74.
[9] Hany N, Hantouche E, Harajli M. Axial stress-strain model of CFRP confined concrete under monotonic and cyclic loading. J Compos Constr, ASCE 2015;19 (6):04015004.
[10] Mirmiran A, Zagers K, Yuan WQ. Nonlinear finite element modeling of concrete confined by fiber composites. Finite Elem Anal Des 2000;35(1):79–96.
[11] Yu T, Teng JG, Wong YL, Dong SL. Finite element modeling of confined concrete – I: Drucker-Prager type plasticity model. Eng Struct 2010;32(3):665–79.
[12] Jiang JF, Wu YF. Identification of material parameters for Drucker-Prager plasticity model for FRP confined circular concrete columns. Int J Solid Struct 2012;49(3–4):445–56.
[13] Eid R, Paultre P. Plasticity-based model for circular concrete columns confined with fibre-composite sheets. Eng Struct 2007;29(12):3301–11.
[14] Karabinis AI, Rousakis TC, Manolitsi GE. 3D finite-element analysis of substandard RC columns strengthened by fiber-reinforced polymer sheets. J Compos Constr, ASCE 2008;12(5):531–40.
[15] Issa C, Chami P, Saad G. Compressive strength of concrete cylinders with variable widths CFRP wraps: experimental study and numerical modeling. Constr Build Mater 2009;23(6):2306–18.
[16] Doran B, Koksal HO, Turgay T. Nonlinear finite element modeling of rectangular square concrete columns confined with FRP. J Mater Des 2009;30(8):3066–75.
[17] Koksal HO, Doran B, Turgay T. A practical approach for modeling FRP wrapped concrete columns. Constr Build Mater 2009;23(3):1429–37.
[18] Wu HL, Wang YF, Yu L, Li XR. Experimental and computational studies on high-strength concrete circular columns confined by aramid fiber-reinforced polymer sheets. J Compos Constr, ASCE 2009;13(2):125–34.
[19] Hajsadeghi M, Alaee FJ, Shahmohammadi A. Investigation on behaviour of square/rectangular reinforced concrete columns retrofitted with FRP jacket. J Civil Eng Manage 2011;17(3):400–8.
[20] Jiang JF, Wu YF. Characterization of yield surfaces for FRP-confined concrete. J Eng Mech, ASCE 2014;140(12):04014096.
[21] Rousakis TC, Karabinis AI, Kiousis PD, Tepfers R. Analytical modelling of plastic behaviour of uniformly FRP confined concrete members. Composites B 2008;39(7–8):1104–13.
[22] Rousakis TC, Rakitzis TD, Karabinis AI. Design-oriented strength model for FRP confined concrete members. J Compos Constr, ASCE 2012;16(6):615–25.
[23] ABAQUS. ABAQUS Theory and User Manuals, version 6.13-1; 2013.
[24] Youssf O, ElGawady M, Mills J, Ma X. Finite element modelling and dilation of FRP-confined concrete columns. Eng Struct 2014;79:70–85.
[25] Yu T, Teng JG, Wong YL, Dong SL. Finite element modeling of confined concrete – II: Plastic-damage model. Eng Struct 2010;32(3):680–91.
[26] Teng JG, Xiao QG, Yu T, Lam L. Three-dimensional finite element analysis of reinforced concrete columns with FRP and/or steel confinement. Eng Struct 2015;97:15–28.
[27] Kabir M, Shafei E. Plasticity modeling of FRP-confined circular reinforced concrete columns subjected to eccentric axial loading. Compos Part B – Eng 2012;43(8):3497–506.
[28] Ozbakkaloglu T, Gholampour A, Lim JC. Damage-plasticity model for FRP-confined normal-strength and high-strength concrete. J Compos Constr, ASCE 2016. http://dx.doi.org/10.1061/(ASCE)CC.1943-5614.0000712, 04016053.
[29] Lo SH, Kwan AKH, Ouyang Y, Ho JCM. Finite element analysis of axially loaded FRP-confined rectangular concrete columns. Eng Struct 2015;100:253–63.
[30] Dong CX, Kwan AKH, Ho JCM. A constitutive model for predicting the lateral strain of confined concrete. Eng Struct 2015;91:155–66.
[31] Menétrey P, Willam KJ. Triaxial failure criterion for concrete and its generalization. ACI Struct J 1995;92(3):311–8.
[32] Lubliner J, Oliver J, Oller S, Oñate E. A plastic-damage model for concrete. Int J Solid Struct 1989;25(3):299–326.
[33] Lee J, Fenves G. Plastic-damage model for cyclic loading of concrete structures. J Eng Mech, ASCE 1998;124(8):892–900.
[34] ACI Committee 318-11/318R-11. Building code requirements for reinforced concrete and commentary. Farmington Hills (MI): American Concrete Institute; 2011.
[35] ASCE Task committee on concrete and masonry structure. State of the art report on finite element analysis of reinforced concrete. ASCE; 1982.
[36] Tao Z, Wang ZB, Yu Q. Finite element modelling of concrete-filled steel stub columns under axial compression. J Const Steel Res 2013;89:121–31.
[37] Popovics S. A numerical approach to the complete stress-strain curve of concrete. Cem Concr Res 1973;3(5):583–99.
[38] Mander JB, Priestley MJN, Park R. Theoretical stress-strain model for confined concrete. J Struct Eng, ASCE 1988;114(8):1804–26.
[39] Papanikolaou VK, Kappos AJ. Confinement-sensitive plasticity constitutive model for concrete in triaxial compression. Int J Solid Struct 2007;44 (21):7021–48.
[40] Teng JG, Huang YL, Lam L, Ye LP. Theoretical model for fiber-reinforced polymer-confined concrete. J Compos Constr, ASCE 2007;11(2):201–10.
[41] Karabinis AI, Rousakis TC. Concrete confined by FRP material: a plasticity approach. Eng Struct 2002;24(7):923–32.
[42] Lim JC, Ozbakkaloglu T. Lateral strain-to-axial strain relationship of confined concrete. J Struct Eng, ASCE 2014;141(5):04014141.
[43] Mirmiran A, Shahawy M. A new concrete-filled hollow FRP composite column. Composites B 1996;27(3–4):263–8.
[44] Spoelstra MR, Monti G. FRP-confined concrete model. J Compos Constr, ASCE 1999;3(3):143–50.
[45] Fam AZ, Rizkalla SH. Confinement model for axially loaded concrete confined by circular fiber-reinforced polymer tubes. ACI Struct J 2001;98(4):451–61.
[46] Lim JC, Ozbakkaloglu T. Investigation of the influence of the application path of confining pressure: tests on actively confined and FRP-confined concretes. J Struct Eng, ASCE 2014;141(8):04014203.
[47] Lim JC, Ozbakkaloglu T. Unified stress-strain model for FRP and actively confined normal-strength and high-strength concrete. J Compos Constr, ASCE 2014;19(4):04014072.
[48] Seow PEC, Swaddiwudhipong S. Failure surface for concrete under multiaxial load – a unified approach. J Mater Civil Eng, ASCE 2005;17(2):219–28.
[49] Lim JC, Ozbakkaloglu T. Stress-strain model for normal- and light-weight concretes under uniaxial and triaxial compression. Constr Build Mater 2014;71:492–509.
[50] Lam L, Teng JG. Ultimate condition of fiber reinforced polymer-confined concrete. J Compos Constr, ASCE 2004;8(6):539–48.
[51] Valdmanis V, De Lorenzis L, Rousakis T, Tepfers R. Behaviour and capacity of CFRP-confined concrete cylinders subjected to monotonic and cyclic axial compressive load. Struct Concr 2007;8(4):187–200.
[52] Wong YL, Yu T, Teng JG, Dong SL. Behavior of FRP-confined concrete in annular section columns. Composites B 2008;39(3):451–66.
[53] Vincent T, Ozbakkaloglu T. Influence of concrete strength and confinement method on axial compressive behavior of FRP confined high- and ultra high-strength concrete. Composites B 2013;50:413–28.
[54] Ozbakkaloglu T. Axial compressive behavior of square and rectangular high-strength concrete-filled FRP tubes. J Compos Constr, ASCE 2012;17(1):151–61.
[55] Ozbakkaloglu T. Behavior of square and rectangular ultra high-strength concrete filled FRP tubes under axial compression. Composites B 2013;54:97–111.